Towards a Generalized TLM Algorithm for Solving Arbitrary Reciprocal and Nonreciprocal Planar Structures

Jifu Huang and Ke Wu

***Abstract*—A generalized transmission line matrix (TLM) algorithm is developed in the frequency domain to tackle arbitrary both reciprocal and nonreciprocal anisotropic waveguiding problems. In particular, the modeling issue for arbitrary planar structures is stressed in this work. A new three-dimensional (3-D) condensed node is used to consider the effect of both electric and magnetic constitutive tensors. Various results indicate how the modal dispersive behavior can be manipulated by changing not only the anisotropic characteristics of the substrate, but also the strip/slot geometry as well as the magnitude and orientation of the applied static magnetic field. The present algorithm is useful for CAD and simulation of a large class of gyrotropic waveguide-based microwave and millimeter-wave circuits.**

I. Introduction

The transmission line matrix (TLM) method is well known for its versatile applicability in the modeling of electromagnetic structures. This technique can be mathematically derived from a direct discretization of time-varying Maxwell's curl equations by applying the central finite-difference and averaging scheme [1], although it can also be constructed from Huygen's principle [2], [3]. We have recently proposed a unified TLM model [4] for the simulation of electrical and optical guided-wave problems. In that model, the symmetrical condensed node (SCN) [5] was used to consider simultaneously the electromagnetic effects of permittivity and permeability tensors of material. However, on the construction of complex elements in the permittivity and permeability tensors such as in the case of magnetized ferrite and plasma, the constitutive parameters are customarily formulated in the frequency-domain. To better accommodate the dispersive properties of both reciprocal and nonreciprocal material-based planar circuits in the TLM formalism, this paper presents a gyrotropic node that is self-consistent with general anisotropy. The use of the proposed node leads to an efficient TLM algorithm that is used in this work to solve a large class of planar structures deposited on various gyrotropic substrates or r-cut sapphire substrate. Results obtained by the present analysis indicate how the modal dispersive characteristics can be controlled by choosing appropriate anisotropic property of substrate, strip/slot geometry and its orientation over the surface of the substrate, as well as the magnitude and orientation of the applied dc magnetic field.

II. Gyrotropic TLM Node in Frequency-Domain

In the following, the rectangular Cartesian coordinate is considered for the theoretical analysis. The tensors $\overleftrightarrow{\varepsilon}$ and $\overleftrightarrow{\mu}$ for an anisotropic medium are conventionally expressed as

$$\overleftrightarrow{\varepsilon} = \varepsilon_0(\varepsilon_{ij}) = \varepsilon_0 \begin{pmatrix} \varepsilon_{xx} & \varepsilon_{xy} & \varepsilon_{xz} \\ \varepsilon_{yx} & \varepsilon_{yy} & \varepsilon_{yz} \\ \varepsilon_{zx} & \varepsilon_{zy} & \varepsilon_{zz} \end{pmatrix},$$

$$\overleftrightarrow{\mu} = \mu_0(\mu_{ij}) = \mu_0 \begin{pmatrix} \mu_{xx} & \mu_{xy} & \mu_{xz} \\ \mu_{yx} & \mu_{yy} & \mu_{yz} \\ \mu_{zx} & \mu_{zy} & \mu_{zz} \end{pmatrix} \tag{1}$$

where $\varepsilon_{ij} = \varepsilon'_{ij} - j\varepsilon''_{ij}$ and $\mu_{ij} = \mu'_{ij} - j\mu''_{ij}$. The imaginary parts represent the electric and magnetic losses. ε_0 and μ_0 are the free-space permittivity and permeability, respectively. The time-harmonic Maxwell's curl equations are

$$\begin{aligned} \nabla \times \vec{H} &= j\omega \overleftrightarrow{\varepsilon} \vec{E} \\ \nabla \times \vec{E} &= -j\omega \overleftrightarrow{\mu} \vec{H} \end{aligned} \tag{2}$$

where $\vec{E} = (E_x, E_y, E_z)^T, \vec{H} = (H_x, H_y, H_z)^T$. To establish a standard TLM formulation, the following equality is used that relates network voltages and currents to the electric and magnetic fields

$$\begin{aligned} &V_x = \Delta x \cdot E_x, \quad V_y = \Delta y \cdot E_y, \quad V_z = \Delta z \cdot E_z \\ &I_x = \Delta x \cdot Z_0 \cdot H_x, \quad I_y = \Delta y \cdot Z_0 \cdot H_y, \quad I_z = \Delta z \cdot Z_0 \cdot H_z \\ &X = x/\Delta x, \quad Y = y/\Delta y, \quad Z = z/\Delta z \end{aligned} \tag{3}$$

where $\Delta x, \Delta y, \Delta z$ are the grid dimensions and Z_0 is the characteristic impedance of free space. Substituting (3) into (2) leads to a set of coupled voltage and current differential equations such as

$$\begin{aligned} \nabla \times \vec{I} &= \overleftrightarrow{C} \vec{I} \\ \nabla \times \vec{V} &= -\overleftrightarrow{L} \vec{V} \end{aligned} \tag{4}$$

where $\vec{V} = (V_x, V_y, V_z)^T, \vec{I} = (I_x, I_y, I_z)^T$ and the elements of two parameter tensors are given in the following:

$$\begin{aligned} &C_{xx} = j\varepsilon_{xx}k_0\Delta y\Delta z/\Delta x, \quad C_{xy} = j\varepsilon_{xy}k_0\Delta z, \\ &C_{xz} = j\varepsilon_{xz}k_0\Delta y \quad C_{yy} = j\varepsilon_{yy}k_0\Delta x\Delta z/\Delta y, \\ &C_{yx} = j\varepsilon_{yx}k_0\Delta z, \quad C_{yz} = j\varepsilon_{yz}k_0\Delta x \\ &C_{zz} = j\varepsilon_{zz}k_0\Delta x\Delta y/\Delta z, \quad C_{zx} = j\varepsilon_{zx}k_0\Delta y, \\ &C_{zy} = j\varepsilon_{zy}k_0\Delta x \quad L_{xx} = j\mu_{xx}k_0\Delta y\Delta z/\Delta x, \\ &L_{xy} = j\mu_{xy}k_0\Delta z, \quad L_{xz} = j\mu_{xz}k_0\Delta y \\ &L_{yy} = j\mu_{yy}k_0\Delta x\Delta z/\Delta y, \quad L_{yx} = j\mu_{yx}k_0\Delta z, \\ &L_{yz} = j\mu_{yz}k_0\Delta x \quad L_{zz} = j\mu_{zz}k_0\Delta x\Delta y/\Delta z, \\ &L_{zx} = j\mu_{zx}k_0\Delta y, \quad L_{zy} = j\mu_{zy}k_0\Delta x \end{aligned}$$

and k_0 is the propagation constant in free space. Now the equivalent nodal voltages V_x, V_y, V_z and loop currents I_x, I_y, I_z are normally determined by applying the same procedure as in [4]. As such, a pair of decoupled matrix equations are found to be

$$\begin{pmatrix} C_x & C_{xy} & C_{xz} \\ C_{yx} & C_y & C_{yz} \\ C_{zx} & C_{zy} & C_z \end{pmatrix} \cdot \begin{pmatrix} V_x \\ V_y \\ V_z \end{pmatrix} = \begin{pmatrix} \Psi_x \\ \Psi_y \\ \Psi_z \end{pmatrix} \tag{5a}$$

$$\begin{pmatrix} L_x & L_{xy} & L_{xz} \\ L_{yx} & L_y & L_{yz} \\ L_{zx} & L_{zy} & L_z \end{pmatrix} \cdot \begin{pmatrix} I_x \\ I_y \\ I_z \end{pmatrix} = \begin{pmatrix} \Phi_x \\ \Phi_y \\ \Phi_z \end{pmatrix} \tag{5b}$$

Manuscript received November 10, 1995; revised April 19, 1996. This work was supported by the National Sciences and Engineering Research Council (NSERC) of Canada.

The authors are with the Poly-Grames Research Center, Department of Electrical and Computer Engineering, Ecole Polytechnique de Montreal, Succ. Centre-Ville, Montreal, Quebec, Canada H3C 3A7.

Publisher Item Identifier S 0018-9480(96)05645-1.

TABLE I
β/k_o VERSUS FREQUENCY AND θ ANGLE FOR A UNIAXIALLY ANISOTROPIC SAPPHIRE SUBSTRATE ($\varepsilon_1 = 9.4, \varepsilon_2 = 11.6, w = h = 0.5$ mm)

	β / k₀ values									Errors compared with the SDA (%)					
Freq.	5 GHz			10 GHz			20 GHz			5 GHz		10 GHz		20 GHz	
Methods	SDA	TD	FD	SDA	TD	FD	SDA	TD	FD	FD	TD	FD	TD	FD	TD
$\theta = 0^0$	2.91	2.96	2.92	2.93	3.02	2.93	3.03	3.11	3.02	0.3	1.4	0.0	3.1	0.3	2.6
$\theta=30^0$	2.86	2.95	2.86	2.88	3.00	2.91	2.96	3.09	3.00	0.0	3.1	1.0	4.2	1.3	4.4
$\theta=60^0$	2.75	2.85	2.76	2.77	2.89	2.80	2.84	2.97	2.88	0.4	3.6	1.1	4.3	1.4	4.6
$\theta=90^0$	2.69	2.75	2.67	2.71	2.80	2.71	2.77	2.87	2.78	0.7	2.2	0.0	3.3	0.3	3.6

in which

$$\Psi_x = 2(V_2^i + V_9^i + V_1^i + V_{12}^i),$$
$$\Psi_y = 2(V_4^i + V_8^i + V_3^i + V_{11}^i)$$
$$\Psi_z = 2(V_5^i + V_7^i + V_6^i + V_{10}^i),$$
$$\Phi_x = 2(V_5^i + V_8^i + V_4^i - V_7^i)$$
$$\Phi_y = 2(V_2^i + V_{10}^i - V_6^i - V_9^i),$$
$$\Phi_z = 2(V_3^i + V_{12}^i - V_1^i - V_{11}^i)$$
$$C_x = C_{xx} + 4, \quad C_y = C_{yy} + 4, \quad C_z = C_{zz} + 4$$
$$L_x = L_{xx} + 4, \quad L_y = L_{yy} + 4, \quad L_z = L_{zz} + 4.$$

The immediate step is to make appropriate averaging of the relevant nodal voltages and loop currents at the center of the node. It yields six pairs of hybrid equations that interrelate reflected and incident voltages. For example, for ports 1 and 12, we have

$$V_1^r = V_x + I_z - V_{12}^i$$
$$V_{12}^r = V_x - I_z - V_1^i. \tag{6}$$

The combination of (5) with (6) leads to a full 12 × 12 nodal scattering matrix that completely describes the scattering property of the gyrotropic FDTLM SCN.

III. NUMERICAL EXAMPLES AND DISCUSSION

To examine computational feature and validity of the proposed gyrotropic node, a TLM algorithm [4] based on this nodal scattering matrix is implemented in the frequency-domain. Our particular interest is to apply the present theory to a large class of planar circuits involving permittivity and permeability tensors.

A. Microstrip and CPW on Sapphire Substrates

A Microstrip line is deposited on a uniaxially anisotropic sapphire substrate as shown in [6]. Propagation constant has been calculated in terms of frequency and orientation of the anisotropy axis. In this case, the tensor is in the form of

$$\vec{\varepsilon} = \varepsilon_0 \begin{pmatrix} \varepsilon_1 \cos^2\theta + \varepsilon_2 \sin^2\theta & (\varepsilon_1 - \varepsilon_2)\sin\theta\cos\theta & 0 \\ (\varepsilon_1 - \varepsilon_2)\sin\theta\cos\theta & \varepsilon_2 \cos^2\theta + \varepsilon_1 \sin^2\theta & 0 \\ 0 & 0 & \varepsilon_1 \end{pmatrix}. \tag{7}$$

With reference to [6], the parameters of structure are defined by $\varepsilon_1 = 9.4, \varepsilon_2 = 11.6, w = h = 0.5$ mm. Table I illustrates β/k_0 versus frequency and θ angle. The results are obtained by using the proposed FDTLM node and the time-domain (TDTLM) node [4] as well as the spectral domain approach (SDA) [6]. The SDA always presents a better accuracy than that of discrete techniques as long as planar structure is considered. In analysis of the microstrip line using the TLM algorithm with frequency- and time-domain nodes, a magnetic wall is placed at $x = 0$. Coordinates of the grid mesh in x- and y-directions are 0, 0.125, 0.25, 0.375, 0.5, 0.63, 0.93, 1.93, 5.0 mm and 0, 0.25, 0.375, 0.5 0.63, 1.0, 2.0, 5.0 mm, respectively. Obviously, the results obtained by the FDTLM node are in better agreement with the SDA than the TDTLM node. This comparison implies that the FDTLM node has satisfactory computational accuracy and convergence for planar circuits.

The low loss and excellent dielectric properties of the sapphire material make it attractive for application in high performance microwave circuits especially high temperature superconductors. Models of analysis are available for the z-cut and m-cut planar geometries [7]. It has been recently suggested that the r-cut microstrip be more attractive for superconductive circuits [8]. However, analysis and design of planar circuits on r-cut sapphire are more difficult because, in this case, the optic axis is not aligned with any of the circuit coordinates. It is instead at an angle of 57.6° with respect to the normal direction of the substrate. Quasistatic characteristics were given in [8] as functions of the strip geometry and its orientation on the surface of the substrate. Dispersion characteristics of microstrip line has been presented in [4] with the time-domain node. To compare the performance of both microstrip line and CPW on the r-cut sapphire substrate, a further calculation has been made for an arbitrarily oriented r-cut CPW as shown in Fig. 1. The permittivity tensor of the sapphire is the same as [4]. Fig. 2 is the dispersion characteristics as a function of the angle ϑ of rotation for the r-cut based CPW ($w/h = 1.52, s/h = 0.455$, and $h = 0.33$ mm), showing a visible influence of the angle ϑ on propagation characteristics. The effective dielectric constant $\varepsilon_{\text{eff}} = (\beta/k_0)^2$ drops into the lowest value at $\vartheta = 90°$. In addition, the ε_{eff} of CPW indicates its more significant dependence on the angle ϑ compared to the counterpart of microstrip line [4]. Such a difference can be explained by the fact that the value of ε_{eff} mainly depends on the transverse field profile of the fundamental mode that is obviously different between the microstrip and CPW.

B. CPW on Ferrite Substrate

Planar structure on a magnetized ferrite substrate presents some distinct advantages such as low fabrication cost and compatibility with two- and three-terminal active devices. In this section, a typical analysis is made for CPW deposited on the surface of a ferrite toroid as shown in Fig. 3, together with theoretical and experimental results for the differential phase shift. It should be noted that in [9] the effect of the ferrite sidewalls was approximately taken into account by using a uniform dielectric layer, which leads to a large discrepancy between calculated and measured curves at higher frequency. In the present analysis, the structure is modeled as two horizontal and two vertical ferrite slabs. The orientation of the magnetized ferrite at the four corners is approximated by a straight orientation of 45° angle with respect to the axis coordinate. Hence, the tensor permeability of ferrite for these relevant regions is modified as the following:

$$\vec{\mu} = \mu_0 \begin{pmatrix} \cos^2\theta + \mu \sin^2\theta & (1-\mu)\sin\theta\cos\theta & j\kappa\sin\theta \\ (1-\mu)\sin\theta\cos\theta & \mu\cos^2\theta + \sin^2\theta & -j\kappa\cos\theta \\ -j\kappa\sin\theta & j\kappa\cos\theta & \mu \end{pmatrix} \tag{8}$$

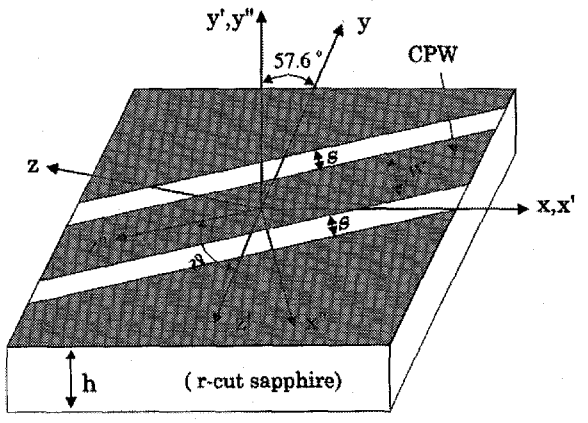

Fig. 1. Arbitrarily oriented r-cut sapphire-based CPW.

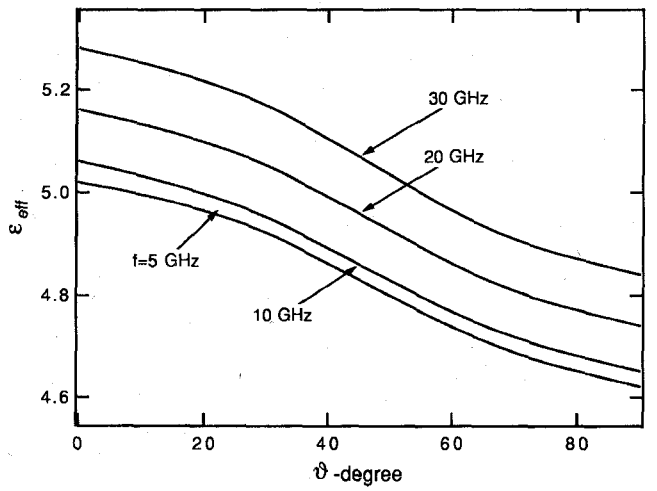

Fig. 2. Propagation characteristics for a CPW deposited on the r-cut sapphire as a function of the arbitrarily oriented angle ϑ ($\varepsilon_1 = 9.4$, $\varepsilon_2 = 11.6$, $w/h = 1.52$, $s/h = 0.455$, $h = 0.33$ mm).

in which

$$\mu = 1 + \frac{\overline{\omega}_0 \omega_m}{\overline{\omega}_0^2 - \omega^2}, \quad \kappa = \frac{\omega \omega_m}{\overline{\omega}_0^2 - \omega^2}$$

$$\omega_m = \tau 4\pi M_s, \quad \overline{\omega}_0 = \omega_0 + j/T, \quad \omega_0 = \tau H_0$$

where ω_0 is the precession frequency, H_0 is the applied dc magnetic field, τ is the gyromagnetic ratio, $T = 2/\tau \Delta H$ is the relaxation time, and ΔH is the 3 dB line width. At corner 1, the angle of rotation is $\theta = 45°$, for instance. The ferrite material used in our calculations is Trans-Tech G-1004 having a normal remnant magnetization of 493 Gauss. The dimensions of the ferrite toroid is taken to be the same as in [9]. It is shown in Fig. 3 that our results are in very good agreement with experiments, considering more realistic physical model of the structure.

C. Microstrip on Magnetized Semiconductor Substrate

It is known that the gyroelectric planar structure is an alternative for developing integrated nonreciprocal devices. In the subsequent section, a study of nonreciprocity for microstrip with magnetoplasmons will be made to show further that the proposed algorithm is versatile with regards to its capability of handling generalized anisotropic layers. A magnetoplasma tensor permittivity was derived in [10] which is characteristic of a magnetoplasma solid-state medium. For

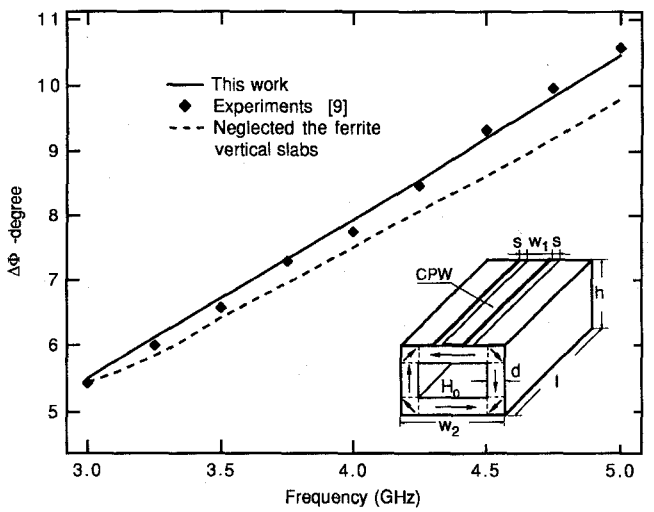

Fig. 3. Differential phase shift of a CPW deposited on the surface of a ferrite toroid (Trans-Tech G-1004 ferrite material, $H_0 = 0$ Oe, $w_1 = 1.6$ mm, $s = 1.0$ mm, $l = 3.2$ cm, $h = 7.1$ mm, $w_2 = 9.9$ mm, $d = 1.6$ mm).

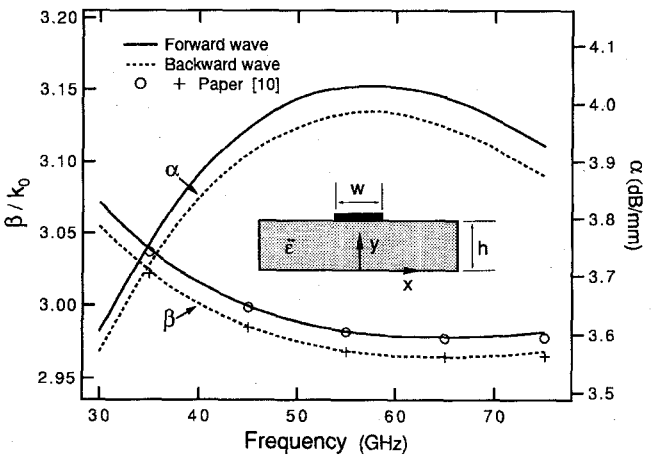

Fig. 4. Dispersion characteristics of a magnetized microstrip line ($\omega_c = 3.925 \times 10^{12}$ rad/s, $\omega_p = 0.628 \times 10^{12}$ rad/s, $\tau_p = 10^{-12}$ s, $\varepsilon_s = 12.5, w = h = 0.1$ mm).

example, for a magnetized microstrip shown in Fig. 4 with the z-directed propagation, when an external dc magnetic field is applied in the x-direction the tensor permittivity becomes

$$\overleftrightarrow{\varepsilon} = \varepsilon_0 \begin{pmatrix} \varepsilon_{xx} & 0 & 0 \\ 0 & \varepsilon_{yy} & \varepsilon_{yz} \\ 0 & \varepsilon_{zy} & \varepsilon_{zz} \end{pmatrix} \tag{9}$$

with

$$\varepsilon_{xx} = \varepsilon_s \left(1 - \frac{\omega_p^2}{\omega(\omega - j\tau_p^{-1})}\right),$$

$$\varepsilon_{yy} = \varepsilon_{zz} = \varepsilon_s \left(1 - \frac{\omega_p^2(\omega - j\tau_p^{-1})}{\omega[(\omega - j\tau_p^{-1})^2 - \omega_c^2]}\right)$$

$$\varepsilon_{yz} = -\varepsilon_{zy} = \frac{-j\varepsilon_s \omega_p^2 \omega_c}{\omega[(\omega - j\tau_p^{-1})^2 - \omega_c^2].}$$

In these equations, ε_s is the relative dielectric constant of the semiconductor, ω_p is the plasma frequency, is the cyclotron frequency, ω_c and the momentum relaxation time τ_p represents the loss mechanism of the semiconductor. The frequency-dependent normalized phase constant β/k_0 and attenuation constant α are also presented in Fig. 4. A very good agreement is observed for β/k_0 with the full-wave SDA

[10]. Also it indicates that the gyroelectric property is similar to that of gyromagnetics.

IV. Conclusion

In this work, a gyrotropic node has been proposed and derived for the TLM technique considering general anisotropy in the frequency domain. An efficient and accurate TLM algorithm using the proposed node has been used to the study of a class of generalized planar structures involving ferrite and semiconductor layers magnetized by applying an arbitrarily oriented external dc magnetic field. The frequency-dependent characteristics of r-cut sapphire-based CPW are also obtained. It is believed that the present field-theoretical modeling technique paves the way to the unified analysis and design of microwave and millimeter-wave integrated nonreciprocal devices and high-Tc superconducting devices.

References

[1] H. Jin, R. Vahldieck, and J. Huang, "Direct derivation of the TLM symmetrical condensed node from Maxwell's equation using centered differencing and averaging," in *1994 IEEE MTT-S Int. Microw. Symp. Dig.*, pp. 23–26.

[2] P. B. Johns and R. L. Beurle, "Numerical solution of 2-dimensional scattering problems using a transmission-line matrix," *Proc. Inst. Elec. Eng.*, vol. 118, no. 9, pp. 1203–1208, Sept. 1971.

[3] W. J. R. Hoefer, "The transmission line matrix method—theory and application," *IEEE Trans. Microwave Theory Tech.*, vol. MTT-33, pp. 882–893, Oct. 1985.

[4] J. Huang and K. Wu, "A unified TLM model for wave propagation of electrical and optical structures considering permittivity and permeability tensors," *IEEE Trans. Microwave Theory Tech.*, vol. 43, pp. 2472–2477, Oct. 1995.

[5] P. B. Johns, "A symmetrical condensed node for the TLM method," *IEEE Trans. Microwave Theory Tech.*, vol. MTT-35, pp. 370–377, Apr. 1987.

[6] J. L. Tsalamengas, N. K. Uzunoglu, and N. G. Alexopoulos, "Propagation characteristics of a microstrip line printed on a general anisotropic substrate," *IEEE Trans. Microwave Theory Tech.*, vol. MTT-33, pp. 941–945, Oct. 1985.

[7] L. H. Lee, W. J. Lyons, T. P. Orlando, S. M. Ali, and R. S. Withers, "Full-wave analysis of superconducting microstrip lines on anisotropic substrates using equivalent impedance approach," *IEEE Trans. Microwave Theory Tech.*, vol. MTT-41, pp. 2359–2367, Dec. 1993.

[8] I. B. Vendik, O. G. Vendik, and S. S. Gevorgian, "Effective dielectric permittivity of r-cut sapphire microstrip," in *24th European Microw. Conf. Proc.*, 1994, pp. 395–400.

[9] E. El-Sharawy and R. W. Jackson, "Coplanar waveguide and slot line on magnetic substrates: Analysis and experiment," *IEEE Trans. Microwave Theory Tech.*, vol. 36, pp. 1071–1079, June 1988.

[10] F. Mesa and M. Horno, "Application of the spectral domain method for the study of surface slow waves in nonreciprocal planar structures with a multilayered gyroelectric substrate," *IEE Proc.-H*, vol. 140, no. 3, pp. 193–200, June 1993.

Electromagnetic Boundary Value Problem in the Presence of a Partly Lossy Dielectric: Considerations About the Uniqueness of the Solution

S. Caorsi and M. Raffetto

Abstract—**This paper deals with the uniqueness of the solution of a boundary value problem defined by specifying the tangential components of the electric field over the closed regular boundary (or the tangential components of the magnetic field over the boundary, or the former components over part of the boundary and the latter components over the rest of the boundary) of a limited region containing a linear dielectric material not lossy everywhere. In particular, the uniqueness of the solution is proved in the case where the dielectric is everywhere linear, homogeneous, and lossless, except for a subregion where the dielectric is lossy, linear but not necessarily homogeneous.**

I. Introduction

Many authors have addressed the problem of the uniqueness of the solution of an electromagnetic boundary value problem. As many different types of problems are important in electromagnetics, a lot of different uniqueness theorems, tailored to the specific applications, have been devised. For example, Müller [1], Harrington [2], Balanis [3], and Collin [4] considered time-harmonic electromagnetic fields, and Stratton [5] dealt with arbitrarily time-varying fields.

As far as time-harmonic electromagnetic fields are concerned, it is well known [2], [3] that the tangential components of the electric field or the tangential components of the magnetic field over the boundary (or the former components over part of the boundary and the latter components over the rest of the boundary) of a domain filled with a linear and everywhere lossy dielectric uniquely determines the solution to the boundary value problem. However, to our best knowledge, nobody has proved the uniqueness of the solution when the boundary conditions are the same as described above but the dielectric is made up partly of a lossless dielectric material and partly of a lossy medium. This paper deals specifically with this problem. In particular, it will be shown that the tangential components of the electric field over the boundary (or the tangential components of the magnetic field over the boundary, or the former components over part of the boundary and the latter components over the rest of the boundary) uniquely determine the solution of the corresponding boundary value problem when the medium within the boundary is linear, homogeneous, and lossless, except for a linear and lossy subregion that may be inhomogeneous. Future efforts will be devoted to the general problem in which the linear and lossless dielectric is inhomogeneous (even with jump discontinuities).

II. Definition of the Boundary Value Problem and Uniqueness of Its Solution

Fig. 1 shows the typical boundary value problem considered in this paper. Ω denotes the region of interest, S is its regular boundary, Ω_σ is the region where the dielectric is linear, lossy but not necessarily homogeneous, and S_σ is the regular boundary of Ω_σ. In $\Omega - \Omega_\sigma$ the dielectric is assumed to be linear, homogeneous, and lossless. The

Manuscript received November 13, 1995; revised April 19, 1996.

S. Caorsi is with the Department of Electronics-University of Pavia, I-27100, Pavia, Italy.

M. Raffetto is with the DIBE-University of Genoa, I-16145 Genoa, Italy.

Publisher Item Identifier S 0018-9480(96)05644-X.